Action potentials initiated by single channels opening in a small neuron (rat olfactory receptor)

Joseph W. Lynch and Peter H. Barry
School of Physiology and Pharmacology, University of New South Wales, Sydney, New South Wales, Australia

ABSTRACT Rat olfactory receptor neurons were enzymatically dissociated and studied with the cell-attached configuration of the patch-clamp technique. Biphasic current waveforms induced across the membrane patch by intracellular action potentials were observed in ~5% of cells studied. In one cell in particular, current injected by the opening of a single channel initiated an action potential in the remainder of the cell each time the channel opened. A conventional type of electrical model of the cell and patch allowed the accurate modeling of cell excitability. The same model was used to explain the shape of the action potential current waveforms induced across the patch. The analysis indicated that the whole cell resistance (R_o) was ~40 GΩ and the membrane capacitance (C_o) was close to the standard value of 1 $\mu F \cdot cm^{-2}$. In addition, the threshold potential change necessary to initiate an action potential (V_{th}) was ~13 mV and a minimum current injection of 1 pA was required to depolarize the cell to spike threshold. When the smaller size of mammalian receptors are taken into account, membrane electrical properties were found to be consistent with those of salamander cells investigated by others using whole-cell recording. The analysis also revealed possible errors in the determination of single-channel conductances and reversal potentials by cell-attached recording from small cells.

INTRODUCTION

Olfactory receptor neurons are extremely sensitive detectors of airborne odorants. Due to their small size, the electrophysiological characteristics responsible for conferring this sensitivity have proven difficult to investigate. Recently, whole cell patch studies have produced a coherent description of amphibian receptor membrane properties (mudpuppy: Dionne, 1987; salamander: Firestein and Werblin, 1987; bullfrog: Suzuki, 1987). Mammalian receptors are smaller and to date have not proven amenable to conventional voltage-clamp or whole-cell patch recording. Consequently, no direct measurements have been made on the passive membrane electrical properties of mammalian olfactory receptor neurons or on their sensitivity to injected current.

During investigations using the cell-attached configuration of the patch-clamp technique, we have observed action potential current waveforms induced across the patch in ~5% of cells, and that the firing rate is increased when current is injected by the opening of single channels. Others have reported similar behavior in olfactory receptor neurons (Frings and Lindemann, 1988; Maue and Dionne, 1987*b*; Trotier and MacLeod, 1987) as well as in other small excitable cell types (chromaffin cells: Fenwick et al., 1982; pancreas beta cells: Ashcroft et al., 1984). In one particular cell, we found that a direct relationship existed between the opening of a channel and the initiation of an action potential in the cell, which was represented as a biphasic current waveform across the patch. This was observed over a wide range of patch pipette potentials. These conditions are necessary to adequately model cell excitability. In this report, we show that it is possible to quantitatively describe the observed excitability features of this cell by the use of a conventional type of equivalent circuit model of the cell and patch. Such a model can also be used to explain the shape of current waveforms induced across the patch by the action potential in the remainder of the cell. The electrical properties thus derived indicate that mammalian olfactory receptors have membrane properties consistent with those of salamander olfactory cells, when differences in cell size are taken into account. This study also reveals possible pitfalls in the determination of single-channel properties by cell-attached recording from any small cell with a high input resistance.

METHODS

Preparation

The method of producing isolated rat olfactory receptor neurons was based on that described by Maue and Dionne (1987*a*). Adult female Wistar rats were killed by CO_2 inhalation. The olfactory epithelia and supporting cartilage were quickly removed and placed in a divalent cation-free solution which contained (in mmol. $liter^{-1}$): NaCl, 137; KCl, 5; $NaHCO_3$, 4; KH_2PO_4, 0.5; Na_2HPO_4, 0.3; glucose, 5.5 (pH 7.4). Olfactory epithelia were then gently separated from the cartilage and placed in 5 ml dissociating solution with a similar formula to that described above, but modified by the addition of 1.75 mg of trypsin (Gibco, Grand Island, NY). The final concentration of trypsin was

0006-3495/89/04/755/14 $2.00

~0.035%. Enzymatic dissociation was achieved by incubating the preparation at 37°C for 30 min while simultaneously applying regular gentle trituration. The dissociation was terminated by adding 1 mg of trypsin inhibitor (Calbiochem-Behring Corp., La Jolla, CA) to the solution and allowing it to stand for ~ 10 min at room temperature. Approximately 2 ml of supernatant was then pipetted into a glass petri dish that had been previously coated with concanavalin A (Maue and Dionne, 1987*a*) to permit cell adhesion. The preparation was left for ~15 min until the cells had precipitated from suspension and adhered to the base of the dish. The superfusion solution was replaced by Hanks' balanced salt solution before the cells were used in experiments. The preparation was viewed with model IMT-2 inverted microscope (Olympus Corp., Tokyo, Japan) using phase contrast optics.

Olfactory receptor neurons isolated by this procedure remained viable for 4–5 h and were easily distinguished by their characteristic morphology. Cell bodies were usually round or ovoid with a diameter of 5–8 μm. A single dendritic process of length 5–30 μm extended from the body and terminated in a small dendritic knob. Cilia protruding from the knob were visible in ~10% of cases. Axonal processes were not observed. However, cilia and axons do not always seem to be clearly resolved by our microscope optics. Only refractile cells with a nongranulated appearance were studied. Our investigations using this preparation have been limited by the inability to obtain stable whole-cell recordings.

Data recording and analysis

Patch pipettes with resistances of 5–10 MΩ were made from borosilicate hematocrit tubing (Modulohm 1/S, Vitrex, Herlev, Denmark) using a two-stage electrode puller (model 720, David Kopf Instruments, Tujunga, CA). Pipettes were then fire-polished and coated with Sylgard (No. 170, Dow Corning, Midland, MI) to within 50 μm of the tip. The solution used to fill the pipette contained (in mmol. liter^{-1}): KCl, 145; $CaCl_2$, 2; $MgCl_2$, 1; NaHepes, 10; glucose, 10 (pH 7.4). The cell-attached configuration of the patch-clamp technique (Hamill et al., 1981) was used and measurements were made using an EPC-7 patch-clamp amplifier (List Medical, Darmstadt, FRG). The experiment was performed at room temperature (22°C). Single channel data were recorded on a Sony video cassette recorder via a digital audio processor. Data were filtered at 1 kHz then digitized at 5 kHz and analyzed using an IBM PC/AT computer. Theoretical analysis programs were written in the Turbo C language, and current records, predicted curves, and other diagrams were plotted on a model 7470A plotter (Hewlett-Packard Co., Palo Alto, CA).

RESULTS

General observations

The data analyzed below were obtained from a single neuron which had a diameter of ~8 μm, a dendritic process ~20 μm long, and no visible axon or cilia. It was investigated at patch pipette potentials varying from −120 to 100 mV. At hyperpolarized membrane potentials (i.e., positive patch pipette potentials), current injected into the cell by the opening of a single channel caused an action potential to be initiated and an action potential current to be recorded across the patch, providing the channel remained open for long enough to charge the membrane capacitance and depolarize the cell interior to threshold potential. The few exceptions to this are discussed below. A typical section of record is shown in Fig. 1. Action potential patch currents were observed at all patch pipette potentials between 10 and 100 mV (at 10-mV increments).

Action potentials occurring either spontaneously or in response to channels opening outside the patch were very rarely observed (one each at pipette potentials of 10 and 30 mV; see below for details). Action potentials were never observed at pipette potentials <10 mV. Each channel opening, regardless of the duration, never initiated more than one action potential. However, long channel openings often seemed to cause slow oscillations of the cell resting potential after the action potential (Fig. 2 *A*). The magnitude of these oscillations diminished slowly with time. Direct recordings of olfactory receptor neuron action potentials (Anderson and Hamilton, 1987; Firestein and Werblin, 1987) have shown that such oscillations are a typical response of olfactory receptor neurons to sustained current injection and that they can reach peak-to-peak amplitudes of at least 20 mV. Brief (< 50 ms) closures of the channel appeared to regenerate oscillation amplitudes, whereas additional channel openings had little effect (Fig. 2 *A*). These observations are consistent with the hypothesis that the oscillations were produced by the synchronous activation of a dwindling fraction of the cell's complement of voltage-activated

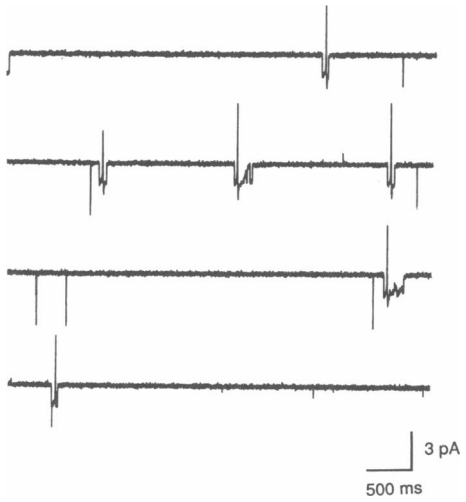

FIGURE 1 Action potential patch-current waveforms initiated by the opening of single channels. In all figures, downward current deflections represent channel openings and currents flowing into the cell. Action potential patch currents (*upward spikes*) in the remainder of the cell were initiated by current injected into the cell by the opening of single channels in the patch. The large downward spikes were large-conductance "bursting" channels with openings too brief to initiate action potentials. The four current records are continuous and were made at a pipette potential of +70 mV. All displayed records were filtered at 1 kHz.

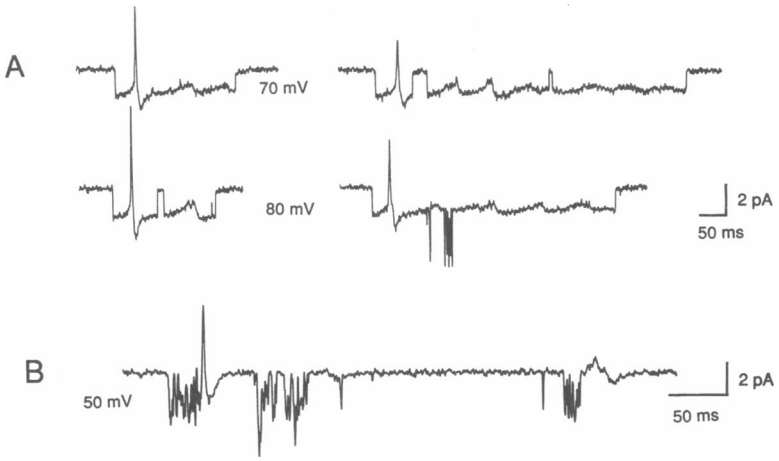

FIGURE 2 Other features of cell excitability as implied by currents recorded across the membrane patch. (*A*) The response of the cell to sustained current injection caused by long-duration channel openings. Slow oscillations of cell internal potential appeared to follow the initial action potential current waveform. Brief closures of the channel increased oscillation amplitude without initiating further spikes (*upper right, lower left traces*). Additional channel openings ("bursting" channels on lower right trace) appeared to have little effect on the oscillation amplitude. The two upper traces were recorded at a pipette potential of 70 mV and the lower two at 80 mV. (*B*) Channels opening <50 ms after an earlier spike failed to produce a further spike. In this case, a particularly strong stimulus (second channel burst) produced a barely detectable response. Channels opening 50–300 ms after an earlier action potential (the third channel burst) elicited an action potential waveform of reduced magnitude and longer time course.

channels, a portion of which were reactivated by brief returns to the resting potential.

Channels opening 50–300 ms after an earlier action potential generally produced action potential current waveforms of diminished amplitude and longer time course (Fig. 2 *B*). Some possible causes of this reduced excitability are considered below (see Discussion).

The patch contained two active channel types, which were easily distinguished on the basis of their conductance and kinetic properties. Examples of each can be seen in Figs. 2 and 4. Current-voltage relationships for both channels are plotted in Fig. 3. The first channel type, characterized by long duration current transitions, had a zero current amplitude at a pipette potential of -10 mV and an apparent chord conductance of 19 pS. Current flow through this channel could not be reversed. These parameters were calculated using the assumption that cell internal potential remained constant as pipette potential was varied. As shown below, this assumption is invalid in the case of very small cells with high input impedances and can lead to large errors. The true chord conductance of this channel was estimated to be ~ 29 pS and the true reversal potential to be ~ -44 mV. It was assumed to be an inwardly rectifying K^+ channel because its conductance, kinetic behavior, and apparent inability to permit outward current flow are consistent with the properties of inwardly rectifying K^+ channels in the olfactory receptor neurons of mice (Maue and Dionne, 1987*b*) and salamanders (Trotier, 1986), as well as in other cell types (e.g., cardiac ventricular cells: Sakmann and Trube, 1984). The second channel type (of which at least two were present) displayed distinctive "bursting" or "flickery" kinetics and had an apparent chord conductance of 35 pS (based on average current peak heights) and the currents reversed at a pipette potential of -36 mV. Current flow

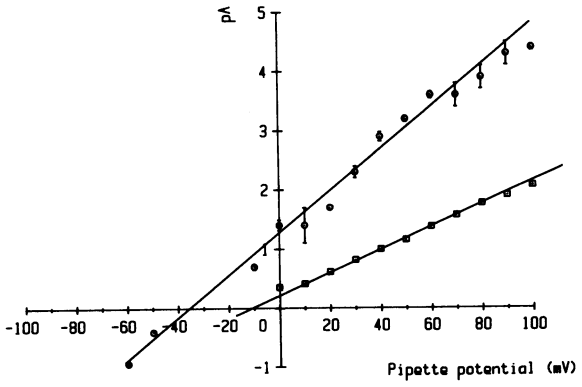

FIGURE 3 Single-channel current-voltage relationships plotted for both the "bursting" channel (*circles*) and the channel with long-duration current transitions (*squares*). Points represent the means of all single-channel events observed at each pipette potential, and error bars (±SEM) are displayed when larger than symbol size. As determined from this graph, the mean apparent slope conductance of the "bursting" channel was 35 pS (fitted by linear regression) and for the long-duration channel was 19 pS. The conductances measured by this means are significantly lower than their calculated true values (52 and 29 pS, respectively) and the pipette potentials corresponding to zero current across the channel are also likely to be incorrect.

through this channel was clearly reversible. Its true chord conductance was estimated to be ~52 pS and may be encompassed by the 83.3 ± 11.5 pS Ca^{2+}-sensitive K^+ channel with similar kinetics described by Maue and Dionne (1987*b*). However, the activity of this channel was not strongly correlated with the purported Ca^{2+} entry during the action potential (see Discussion).

Initiation of action potentials by single-channel openings

This section deals only with the analysis of events between the opening of the channel and the initiation of the action potential. Only action potential current waveforms occurring in response to the opening of square (29 pS) channels were analyzed. Action potentials associated with the "bursting" channels were excluded because single-channel currents could not be accurately measured and the trends of currents preceding action potentials were obscured.

As seen in Fig. 4, when the pipette potential was increased, the latency between the opening of the channel and the initiation of the action potential current waveform was reduced. This time, plotted as a function of pipette potential, is displayed in Fig. 5 *A*. Another feature, also apparent in Fig. 4, is that the current level of the open channel declined steadily until the point of action potential initiation. The magnitude of this decline at the point of action potential initiation, expressed as a percentage of the initial current level of the open channel, was also a function of pipette potential. This has been defined as "current droop" and is displayed as a function of pipette potential on Fig. 5 *B*. A third feature is that the total charge required to produce an action potential (where charge equals area under the current trace between channel opening and initiation of the action potential patch current) was also reduced as pipette potential was increased. Such values of charge are plotted against pipette potential in Fig. 5 *C*.

Some limitations of these data values are recognized. At low rates of current injection (i.e., low pipette potentials) some degree of Na^+ channel inactivation may occur, thus reducing the action potential depolarization rate. Evidence that this may have occurred is that at pipette potentials of 10 and 20 mV, action potential current waveforms were smaller than those at higher pipette potentials (see Fig. 4). Data for pipette potentials of 10, 20, and 30 mV were recorded at the beginning of the patch record. Action potential patch currents (one each) at pipette potentials of 10 and 30 mV (see Fig. 4) were observed without channel openings. The one at 30 mV occurred at the end of the recording for that potential. A channel opening elsewhere in the cell and staying open for the remainder of the recording would not only explain

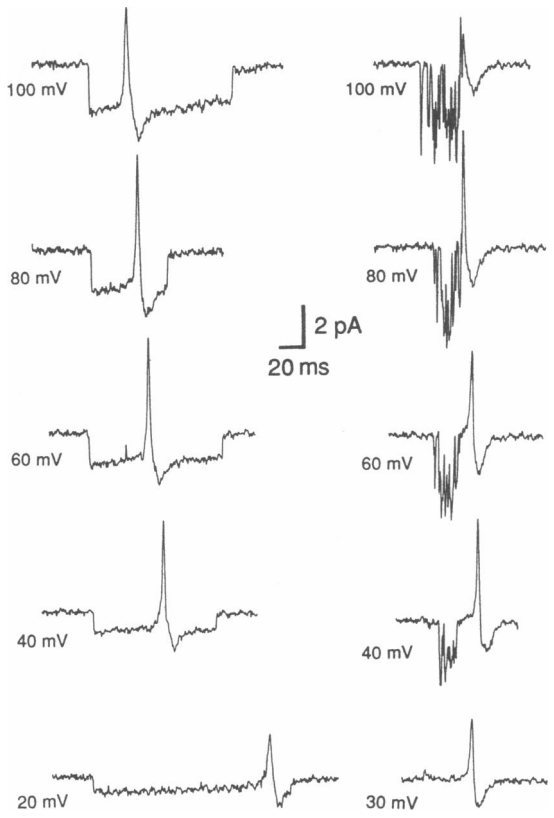

FIGURE 4 Changes in cell excitability with pipette potential and differences in action potential patch-current waveform shapes between the channel being open and closed. The patch pipette potential is indicated for each trace. In the left column it can be seen that the latency between the opening of a single channel and the initiation of an action potential patch current is reduced as pipette potential (hence rate of current injection) is increased. The righthand column shows action potential patch currents that happened to be initiated shortly before the closure of "bursting" channels at similar pipette potentials. They are included to show the difference between the shape of action potential patch currents when the channel is open and closed. Note the reduced size of action potential patch currents at pipette potentials of 20 and 30 mV, which were presumably the result of Na^+ channel inactivation caused by low current injection rates. The action potential waveform at 30 mV was one of only two that occurred without a channel opening in the patch and was probably initiated by a channel opening outside the patch.

this particular action potential, but would also provide a rationale for the data recorded later at higher pipette potentials (40–100 mV) being consistent with a lower whole cell resistance than the data recorded at 30 mV. Finally, at pipette potentials of 10 and 20 mV, prolonged channel openings occasionally did not elicit action potential patch currents, although slow potential oscillations (similar to those in Fig. 2 *A*) were observed. It is interesting to note that when the mathematical model of cell excitability developed in Appendix A is used, small variations in cell and patch electrical constants cause proportionately larger variations in cell excitability at low

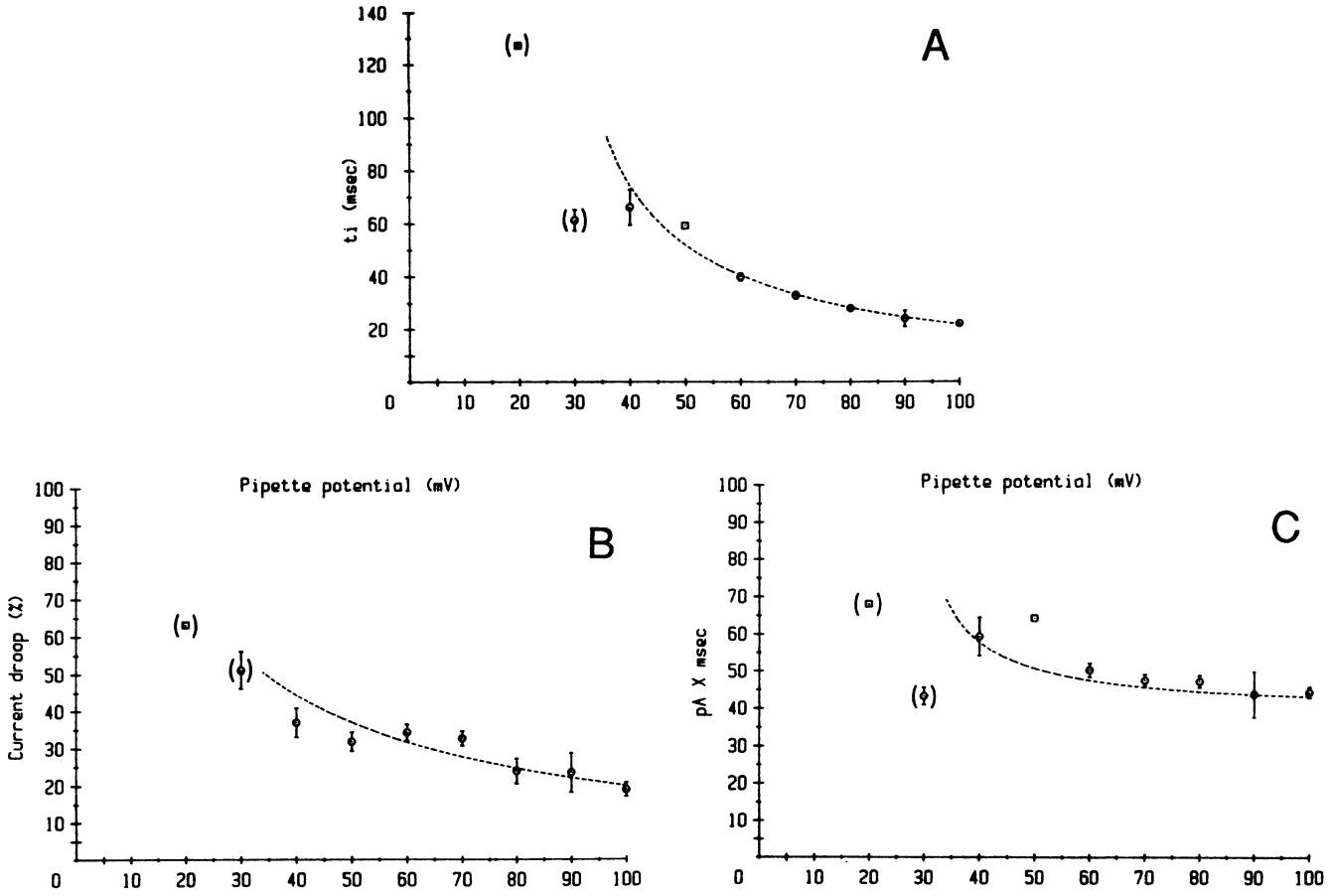

FIGURE 5 Features of cell excitability plotted as functions of patch pipette potential. In each case, the action potential initiation point was taken as the initial inflection in the current trace immediately preceding the initial spike. Circles are the averages of multiple points and error bars (±SEM) which are larger than symbol size are displayed. Squares represent single data values. Symbols enclosed in brackets represent data of questionable significance (see text). Dashed line curves represent the prediction of the model (see Appendix A) in describing the excitable properties of the cell. (*A*) The time (t_i) elapsed between the opening of a square (29 pS) channel and the initiation of an action potential plotted as a function of pipette potential. (*B*) "Current droop" plotted as a function of pipette potential. Current droop is the magnitude of the open channel current level at the point of action potential patch current initiation, expressed as a percentage of the initial open channel current level. (*C*) The charge required to initiate an action potential plotted as a function of pipette potential. Charge was defined as the area beneath the current-time curve between the opening of the 29 pS channel and the initiation of the action potential.

pipette potentials. Also, because the data at pipette potentials of 10, 20, and 30 mV were recorded first, we are inclined to suspect that the cell took some time to reach a steady electrical state after establishment of the gigaohm seal. Because of these variations in cell excitability at low current injection rates, little effort was made to model the data recorded at pipette potentials of 10, 20, and 30 mV.

However, at pipette potentials of >30 mV, trends were quite consistent and anomalies such as those described above were never observed. Hence we feel justified in fitting models accurately to data recorded between 40 and 100 mV.

An electrical model of the situation, a slight extension of that described in Fenwick et al. (1982), is shown in Fig. A1. In Appendix A, equations are derived from which it is possible to determine expressions for time and charge required for the initiation of an action potential and for the magnitude of the current droop at the point of action potential current initiation. A specific aim of the paper has been to determine whether the substitution of realistic values of cell and patch parameters into these equations can simulate the observed characteristics of cell excitability displayed in Fig. 5, *A–C*.

The dashed line curves superimposed onto the data in Fig. 5, *A–C* were produced when the following quantities were substituted into the model developed in Appendix A.

$R_p = 110$ GΩ; $R_o = 40$ GΩ; $\gamma_c = 29$ pS;

$C_o = 3$ pF; $C_p = 0.2$ pF; $E_R = -70$ mV;

$E_c = -44$ mV; $V_{th} = 13$ mV; $E_D = 0$ mV.

These terms are defined below and in Fig. A1 and Appendix A. Each parameter was restricted to a narrowed range of values estimated from cell size and published values of these parameters for olfactory receptor neurons. The final value was then determined more accurately by trial and error fitting of the model to the data. These quantities and the limitations of their accurate fitting are now discussed.

Patch resistance (R_p)

The total seal conductance was determined from the change in baseline current with pipette potential and found to be 19 pS (53 GΩ). As indicated by Fenwick et al. (1982), this is the sum of the leakage conductance around the seal ($1/R_s$) and the leakage conductance through the patch ($1/R_p$). Hence R_p must be >53 GΩ.

Whole cell resistance (R_o)

For a single channel to depolarize the cell interior, its resistance must be of comparable magnitude to the whole cell resistance to produce an effective shunt to ground. As expected, the ratio R_p/R_o was the main factor determining current droop (Fig. 5 *B*), and variation outside the range 2–4 precluded an accurate fit to the data irrespective of how other quantities were varied to compensate. These factors imply a whole cell resistance well into the gigaohm range. The total cell surface area, when approximated as a sphere of diameter 8 μm and a cylinder 20 × 1 μm, was ~270 μm^2. With the empirically determined R_o of 40 GΩ, this yields a specific membrane resistance of ~1.1×10^5 Ω cm^2, very similar to that found in amphibian receptor cells (10^5 Ω cm^2; Firestein and Werblin, 1987). Note that a valid extimate of R_o may not necessarily be gleaned by assuming that the ratio R_o/R_p is approximated by the ratio of patch area to total cell area. Fenwick et al. (1982) presented evidence that the membrane patch may be slightly disrupted during the formation of a gigaohm seal resulting in a comparatively low value of R_p. Also, Fischmeister et al. (1986) found that R_p depended on the composition of the pipette solution.

Single-channel conductance (γ_c) and channel reversal potential (E_c)

Based on the assumption of constant cell internal potential, the apparent chord conductance appeared to be ~19 pS (see Fig. 3). The reversal of currents at a pipette potential of −10 mV, implied an apparent reversal potential of −60 mV (assuming a membrane potential of −70 mV) across the channel. However, at positive pipette potentials, charge is injected into the cell through the patch resistance (R_p). In the case of very small cells with high input impedances, this is sufficient to significantly depolarize the cell interior. At a pipette potential of 100 mV, with the parameters listed above, the resting potential is actually depolarized by 45 mV without the opening of any channels in the patch. This clearly reduces the driving force across the channel, causing errors in single channel conductances and reversal potentials that are determined by cell-attached recording. The derivation of equations to predict the true conductance and reversal potential are given in Appendix B. In the present case, the true single-channel conductance (γ_c) was calculated to be 29 pS and the true reversal potential (E_c) was calculated to be −44 mV. Fischmeister et al. (1986) employed a different analysis to determine that single-channel conductances were significantly underestimated in cells with high input resistance.

Whole cell capacitance (C_o)

Because amphibian olfactory receptor neuron membranes have been found to have approximately the standard capacitance value of 1 μF cm^{-2} (Dionne, 1987; Firestein and Werblin, 1987; Suzuki, 1987) and assuming a surface area of 270 μm^2, C_o should have been ~2.7 pF. C_o is obviously a major factor determining the charge required to initiate an action potential (Fig. 5 *C*) and it was found that a value of 3 pF produced an accurate fit of the model to the data.

Patch capacitance (C_p)

The ratio C_p/C_o should be approximated by the ratio of patch area to total cell surface area. C_p is not an important determinant of cell excitability, hence its value cannot be accurately estimated by fitting the model to the data in Fig. 5. However, as will be shown below, C_p is an important factor in determining the shape of the currents recorded across the patch in response to action potentials in the cell. Hence, the value of C_p determined below was used here. Given the margin of error for C_p, a ratio of patch area to total cell surface area of the order 0.01–0.1 is predicted.

Cell resting potential (E_R)

The assumed value of cell resting potential (in the absence of depolarization caused by the pipette potential) could be varied between −50 and −120 mV without significantly affecting cell excitability. A value of −70 mV was chosen to be consistent with recent estimates of olfactory receptor neuron resting potentials (Firestein and Werblin, 1987; Suzuki, 1987). However, as shown above, the actual cell resting potential is significantly depolarized as pipette potential is increased.

Threshold potential (V_{th})

This was defined relative to the steady-state value of cell membrane potential at a particular patch potential and clearly has an important effect on cell excitability. Variations outside the range 11–14 mV precluded accurate fit of the model to the data, regardless of how other parameters were varied. This value (13 mV) is consistent with the threshold potential in mature salamander olfactory receptor neurons of 21 ± 10 mV (Hedlund et al., 1987).

Patch diffusion potential (E_D)

This was assumed to be 0 mV, because the composition of the patch pipette solution was essentially the same as that expected for the internal composition of the cell. Choosing a different value did not significantly vary the parameters of best fit.

The final values of the quantities listed above were determined to a certain extent by trial and error and should be considered as first order approximations to the range of values providing acceptable fits to the data. As stated above, exceptions to this are the cell resting potential (E_R), patch capacitance (C_p), and patch diffusion potential (E_D) which could be varied over a wider range with little detriment to the fit. The other parameters, however, could only be varied within a small range ($\sim \pm 20\%$) and there was only a very limited ability for other data to compensate for the effect of moving a data value outside this range. Hence it is considered that these parameters provide useful approximations to actual cell parameters.

Shape of action potential patch-current waveforms

Action potentials in the remainder of the cell induced biphasic current waveforms across the membrane patch. These waveforms were characterized by a large initial spike with current flowing out of the cell and into the patch pipette, followed by a smaller rounded spike with current flowing in the reverse direction and into the cell. In Fig. 4 it can be seen that action potential patch-current waveforms were often recorded shortly after the closure of higher conductance "bursting" channels and that these generally had smaller initial (outward) spikes and larger second spikes than those associated with open channels. These features did not appear to vary with pipette potential (apart from a marked reduction in spike amplitude at low pipette potentials, which can be explained in terms of Na^+ channel inactivation). At all pipette potentials there was a large scatter in waveform spike amplitudes which only allows broad generalizations about patch parameters and waveform shapes to be made from any mathematical model. As discussed below, this problem was exacerbated by the inability to directly record cellular action potentials with their current waveforms induced across the patch. Accordingly, the aim of this section was simply to show that the shape of biphasic current waveforms in response to action potentials can be understood by modeling the membrane patch by an extension of the model used above to explain the initiation of the action potential by the channel.

Fig. C1 is a simplification of Fig. A1 containing only those parameters relevant to determining current waveform shape. The mathematical model for the change in current across the patch induced by a voltage change in the cell is derived in Appendix C.

Because it was not possible to establish the whole-cell recording configuration, direct recordings of action potentials could not be made. Instead, a "typical" action potential was emulated digitally and used in the model derived in Appendix C. Action potentials in vertebrate olfactory neurons have a maximum rising phase of 60–70 $V\ s^{-1}$ (mean slope 30 $V\ s^{-1}$) and overshoot 0 mV by 15–20 mV (Anderson and Hamilton, 1987; Firestein and Werblin, 1987; Suzuki, 1987). The action potential in Fig. 2 *A* in Anderson and Hamilton (1987) was digitized into 84 points between threshold potential and a point past the afterhyperpolarization. When the interpoint interval was adjusted so that the maximum rising phase was 16 $V\ s^{-1}$ and the maximum overshoot was 20 mV, action potential patch current waveforms were found to have similar time courses to those recorded (Fig. 6). If a maximum slope of 60 $V\ s^{-1}$ was employed, the predicted action potential current waveforms were three to four times faster than were actually recorded in this study. The slower action potential time course was probably a consequence of the cell already being substantially depolarized before the action potential was initiated. Anderson and Hamilton (1987) found that hyperpolarizing the membrane potential increases the action potential depolarization rate in olfactory receptor neurons. Hence the action potential depolarization rate appears to be influenced by the degree of Na^+ channel inactivation in these cells.

With this simulated action potential and the same values of electrical constants as used in the previous section, the model predicts action potential current waveforms for a pipette potential of 60 mV as displayed in Fig. 6. Examples of recorded action potential current waveforms are included for comparison. Action potential waveforms recorded at a patch pipette potential of 60 mV were chosen to compare with the predicted waveforms because it was midrange in the data and contained the largest population of action potential current waveforms observed at any potential. At this pipette potential, the initial (outward) peak had a maximum current of 4.7 ±

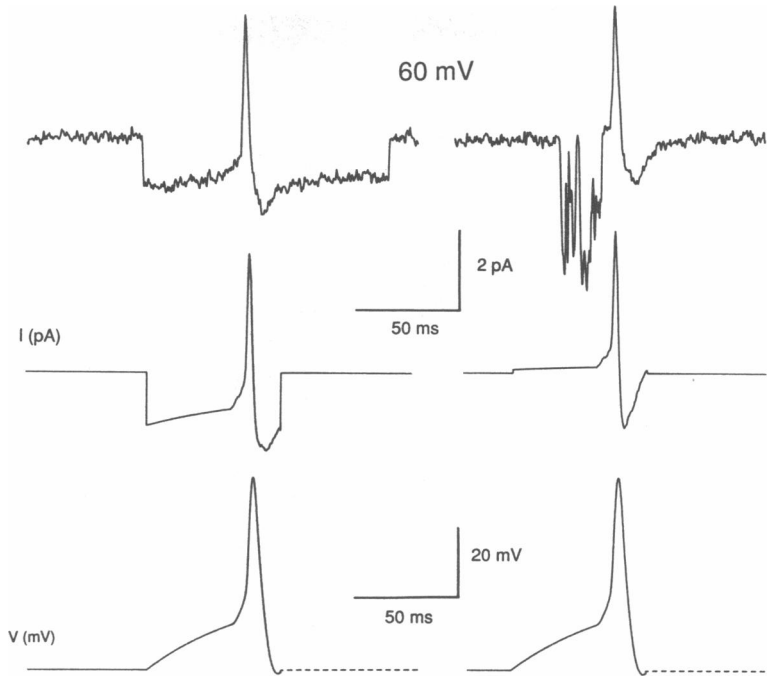

FIGURE 6 Examples of measured and predicted action potential patch-current waveforms for a pipette potential of 60 mV. Two upper traces show action potential current waveforms induced across the patch when the channel is open (*left*) and closed (*right*). Shown beneath these are the respective current waveforms as predicted by the model derived in Appendix A and C when substituted with the parameters determined in the text. Bottom traces show the action potential voltage waveforms used in the model. The main features of the current waveforms are predicted by the model. The action potentials in each case were assumed to be initiated by equal rates of current injection. The action potential trace is completed by a dashed line because its actual time course after this point is not important for the purpose of this model.

0.4 (SEM, $n = 6$) pA when the channel was open (measured from initial open channel current level) and 3.5 ± 0.3 (SEM, $n = 13$) pA when the channel was closed (measured from current baseline). By comparison, the predicted action potential had maximum outward peaks of 4.5 pA and 3.5 pA when the channel was in the open and closed states, respectively. The second (inward) peak had measured maximum currents of 0.7 ± 0.1 (SEM, $n = 9$) pA when the channel was open, and 1.1 ± 0.2 (SEM, $n = 10$) pA when it was closed. The model predicted values of 0.7 and 1.3 pA, respectively. Thus measured and predicted current peak heights are in close agreement.

As seen in Fig. C1, the action potential induces a voltage change across the patch resistance, the channel conductance (when in the open state) and the patch capacitance. For simplicity, consider only the rising phase of the action potential where the total voltage increase is given by V_{max}. From Eq. B5, the change in total current flowing through the patch becomes

$$\Delta i_T = V_{max}/R_p + V_{max} \cdot \gamma_c + C_p \cdot dV(t)/dt. \quad (1)$$

In the present case when the channel is open, the approximate contributions to the first (outward) current peak from these three components are 0.5, 1.5, and 3.2 pA, respectively. Because the capacitative current constitutes the largest component, the effect of the membrane patch is largely to differentiate the action potential voltage curve. Consequently, small variations in the action potential shape can cause significant variations in the shape and amplitude of current waveforms across the patch.

A value of C_p was chosen so that the initial peaks of both the model and the data were consistent. As seen in Eq. 1, such a value of C_p cannot be determined accurately by this means because none of the other quantities are precisely known. γ_c and R_p can be determined with reasonable accuracy (±20%) as discussed above. Both V_{max} and $dV(t)/dt$ are unlikely be in error by $>\pm 50\%$. However, when these errors are compounded, it can be appreciated that the fitted value of C_p is little better than an "order of magnitude" approximation.

The model predicts that the initial outward current peaks of the action potential current waveform are gradually reduced as the pipette potential is increased. The decline is approximately linear, decreasing from 4.9 pA at a pipette potential of 40 mV, to 3.4 pA at 100 mV when the channel is open. Since the cell internal potential is steadily depolarized as pipette potential is increased and

overshoot potential is assumed to remain constant, the voltage change (V_{max}) is progressively reduced. As seen in Eq. 1, this reduces the resistive current components causing the progressively smaller current spikes. This model did not consider the possibility of further increasing Na^+ channel inactivation as the cell is depolarized, which was proposed by Fenwick et al. (1982) to explain the decline in current peak height that they observed with increasing pipette potential. We also observed a reduction in peak currents at pipette potentials of 90 and 100 mV which may be due to this. However, between 40 and 80 mV no such trend was observed. A possible reason is that as the stimulus intensity (i.e., pipette holding potential) was increased, the rate of rise of the action potential became faster. This would have increased the capacitative current component (see Eq. 1) and kept the magnitude of the initial current peak approximately constant.

DISCUSSION

In this paper, we have shown that the opening of a single ionic channel can directly initiate an action potential in a small excitable cell. The condition under which this occurred was artificial in that an abnormal driving force and external K^+ concentration enhanced the rate of current injection. However, in physiological conditions a similar current (1 pA) could be generated by the opening of one nonselective cation channel with a conductance of at least 14 pS. The possible absence of cilia was not considered to have significantly enhanced cell excitability by increasing whole-cell resistance because of their small diameter (0.2 μm: Getchell, 1986; Lancet, 1986) and probable short length constants. We have also shown that a conventional type of equivalent circuit model of the cell and membrane patch, substituted with realistic electrical parameters, can quantitatively explain the observed features of cell excitability. A similar electrical model can also explain the shape of the current waveforms induced across the membrane patch by the action potential. However, as outlined above, without direct concurrent measurement of individual action potentials it is not possible to model these waveforms more accurately.

If the cell and patch electrical parameters determined above were modified to describe a salamander olfactory neuron with seven times the surface area (Firestein and Werblin, 1987), with the assumption that the membrane parameters per unit area were no different, most parameters would be unchanged except that the whole-cell resistance would be 5.7 GΩ, the whole cell capacitance would be 21 pF and the minimum injected current to reach spike threshold would be 3.5 pA. These compare well with quantities of 5 GΩ, 20 pS, and 3 pA determined by Firestein and Werblin (1987) as being typical for salamander receptors. Assuming amphibian and mammalian neurons share similar membrane properties, this suggests that the neuron investigated in this study had a sensitivity representative of mammalian olfactory receptor neurons. The fact that action potentials initiated by single channels are rarely observed in cell-attached patches is probably due to the spike generating section of the axon being normally severed during cell preparation.

A short term (~300 ms) reduction in cell excitability was invariably observed to follow each action potential (Fig. 2 *B*). Because the inward voltage-gated conductance contains a Ca^{2+} component (Trotier, 1986; Dionne, 1987; Firestein and Werblin, 1987; Suzuki, 1987), the activation of a Ca^{2+}-gated K^+ conductance may have contributed to the reduced cell excitability. Changes in ionic concentration gradients in the cell soma were unlikely to have been responsible because the amount of charge entering the cell during an action potential was calculated to cause concentration changes of <0.01 mM. However, concentration changes would be ~1 mmol · liter^{-1} in the spike generating section of the axon (diameter 0.1 μm), which may have contributed to transient depressed excitability (Gesteland, 1986, 1988) but seems unlikely to have been the major factor. It should be noted that this effect would be more important in vivo, where extracellular concentration changes are relevant and where odorant information is often coded in spike bursts (Frings and Lindemann, 1988). A similar process may be expected in the olfactory receptor cilia where local ionic concentration changes may result from sustained odorant-stimulated currents. These mechanisms may explain the desensitization of olfactory receptor neurons to sustained odorant stimulation (Getchell and Shepherd, 1978; Getchell, 1986).

Fenwick et al. (1982) and Fischmeister et al. (1986) noted that the opening of a single channel can dramatically change the internal potential of a very small neuron. This provides an explanation for the irregular current baseline and random spiking that typify whole-cell recordings from salamander olfactory receptor neurons (Anderson and Hamilton, 1987; Frings and Lindemann, 1988). A high basal rate of spiking would also be a feature of smaller mammalian receptors which are much more sensitive to current injection. Also, this same sensitivity would allow these cells to detect single odorant molecules gating single channels, as earlier predicted by Moulton (1977).

It appears that single spikes produced by a sufficiently small number of odorant-activated cells would not be detected by higher neural circuitry as variations in the spontaneous spiking rate. If these low signal strengths are not detected, what is the rationale for the extraordinary sensitivity of these cells? We suggest that low peripheral signal strengths may be improved if odorants produced

bursts of spikes rather than single spikes. Spike bursts would not usually be initiated by spurious channel openings but may be the result of sustained depolarizations produced either by the direct odorant gating of large or multiple conductance-state channels (Labarca et al., 1988) or by channels activated by second messenger amplification systems (see Nakamura and Gold, 1987; and reviews by Anholt, 1987; Lancet and Pace, 1987). Alternatively, odorant-activated second messenger systems may directly modulate the activity of channels responsible for repetitive spiking behavior. The notion of peripheral olfactory information being coded in bursts is consistent with the observation by Firestein and Werblin (1987) that receptor spiking activity is not finely graded with stimulus intensity. Thus stimulus intensity may be coded by some other means.

Our analysis supports the finding of earlier studies (Fenwick et al., 1982; Fischmeister et al., 1986) that the current injected via the patch resistance into a small cell with high input impedance is sufficient to cause significant depolarization. In the case discussed above, it was calculated that increasing the pipette potential from 0 to 100 mV depolarized the cell from a resting potential of −70 to −25 mV. This can lead to the underestimation of single-channel conductances and errors in the reversal potential of channels studied in the cell-attached patch-clamp configuration. It may explain the discrepancy reported by Maue and Dionne (1987*b*) between the conductance of a K^+ channel in mouse olfactory receptor neurons of 20.6 ± 9.4 pS when cell-attached and 29.4 ± 11.4 pS when excised. This compares remarkably well with a similar channel in the present study which had an apparent measured cell-attached conductance of 19 pS and a true corrected conductance of 29 pS. Similarly, large errors in the reversal potential may result when determined by cell-attached recording. For example, the same channel had an apparent reversal potential of −60 mV and a true corrected reversal potential calculated to be −44 mV.

The opening of single channels rapidly depolarize the cell. These cause current relaxations (described above as "current droop") which follow an exponentially decaying time course. From Eq. A25,

$$\frac{\Delta i_T(t)}{\Delta i_T(0)} = \frac{1 - [1 - (1 + \alpha)R_o C_o/\tau]\, e^{-(1+\alpha)t/\tau}}{(1 + \alpha)\, R_o C_o/\tau}, \quad (2)$$

where, from Eqs. A11,

$$\alpha = (R_o/R_p) + (R_o\gamma_c) \quad (3)$$

and

$$\tau = R_o(C_o + C_p). \quad (4)$$

Hence the time constant for the "on" current relaxation is given by

$$\tau_{on} = (C_o + C_p)/(1/R_o + 1/R_p + \gamma_c), \quad (5)$$

and similarly the "off" current time constant is

$$\tau_{off} = (C_o + C_p)/(1/R_o + 1/R_p). \quad (6)$$

If $C_p \ll C_o$, Eqs. 5 and 6 simplify to

$$\tau_{on} \approx C_o/(1/R_o + 1/R_p + \gamma_c), \quad (7)$$

and

$$\tau_{off} \approx C_o/(1/R_o + 1/R_p). \quad (8)$$

Eqs. 7 and 8 were used by Fenwick et al. (1982) who measured time constants of relaxations from large conductance channel transitions and thereby determined cell and patch electrical constants. In the present case, the channel conductance (γ_c) was too small to clearly show these relaxations. However, they have been observed in other olfactory receptor neurons in response to large conductance channel transitions (our own unpublished observations).

Finally, the results presented here suggest that the determination of cell and patch electrical constants by the modeling of cell excitability provides a verification to constants determined by others using whole-cell patch recording.

APPENDIX A

Derivation of equations describing initiation of an action potential after the opening of a single cation channel in a very small cell by the opening of a single cation channel in a membrane patch

The aim of this appendix is to derive the change in membrane potential of a very small cell, resulting from the opening of a cation channel in a membrane patch on the cell, to determine the conditions that will result in the initiation of an action potential. This will involve derivations of the current and cell depolarization resulting from the pipette potential before and after the channel opens and, where appropriate, the time taken to reach action potential threshold after the channel has opened.

The electrical circuit of the patch and cell (see Fig. A1) will be assumed to be similar to that of Fenwick et al. (1982), except that both the patch capacitance (C_P) and the patch diffusion potential (E_D) will be included. As indicated in Fig. A1, R_P and C_P refer to the patch resistance and capacitance; γ_c, $R_{\gamma c}$, and E_c refer to the conductance, resistance, and null potential of the cation channel; R_o and C_o refer to the resistance and capacitance of the rest of the cell; E_D is the diffusion potential across the patch with the channel closed; R_s is the pipette-patch seal resistance, and i_s is the current through it; V_P is the voltage applied to the patch pipette, and V is the voltage of the cell interior; i_T is the total current being measured by the patch amplifier; i_P, i_{Pc}, and i_c are the currents "through" R_P, C_P, and γ_c, respectively, and i_{Ro} and i_{Co} are the currents

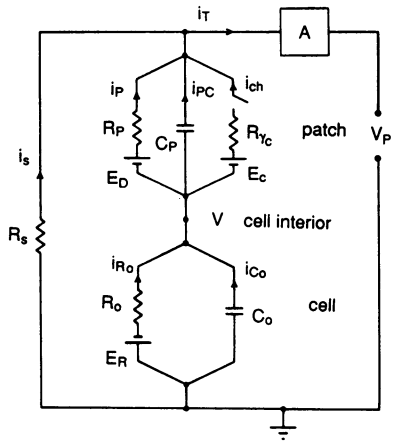

FIGURE A1 A schematic diagram of the full electrical circuit of a small cell and membrane patch with a channel that can be in either an open or closed state. The symbol A represents the patch-clamp amplifier. The subscripts P, ch, s, and o refer to the membrane patch, the channel, seal around the patch pipette and rest of the cell, respectively. E_R, E_D, E_c, and $R_{\gamma c}$ represent the resting potential of the cell, the diffusion potential across the patch, the null potential of the cation channel in the patch and the resistance of the single channel with conductance (γ_c). V_P represents the potential applied to the patch pipette. For further details see Appendix A. The positive directions of the current are as defined by the arrows in the diagram. The circuit is somewhat similar to Fenwick et al. (1982) except that they did not include E_D and C_P in the patch and the leakage resistance of the seal R_s.

"through" R_o and C_o, respectively. All potentials are conventionally defined with respect to the external solution.

Firstly, the steady-state background current and depolarization that results from an increase in pipette potential, V_P, in such a small cell, with the cation channel closed, will be derived. This will be followed by a derivation of the steady-state current, i_P, across the patch, and hence the total background current, i_T^b. When the cation channel opens in the patch (time, $t = 0$), an inward (into the cell) current will result, which will significantly depolarize these small cells and, in turn, decrease the current through the channel and the rest of the patch. The time dependence of this depolarization and decrease in current across the patch will then be derived. Finally, for values of V_P for which the membrane depolarization reaches the threshold for action potential initiation, the duration of channel opening necessary to reach this value, t_i, will be derived.

Derivation of background current and initial cell potential, before channel opens, due to V_P. It will be assumed that the cell is initially at the resting potential, E_R. When the pipette potential, V_P, is applied, there will be a background current through the patch-clamp amplifier (due to leakage current through the seal, i_s, and across the rest of the patch, i_P). This will change the potential across the rest of the cell, tending to depolarize it as V_P is increased. This current, i_T^b, (for $t < 0$), will be given by

$$i_T^b = i_T(t < 0) = -\{[(V_P + E_D - E_R)/(R_P + R_o)] + [V_P/R_s]\}, \quad \text{(A1)}$$

which can be written as

$$i_T^b = i_s - \delta[V_P + E_D - E_R]/[R_o(1 + \delta)], \quad \text{(A2)}$$

where

$$\delta = R_o/R_P, \quad \text{(A3)}$$

and where the current directions are as indicated in Fig. A1.

The initial background voltage across the rest of the cell will be given by

$$V^b = V(t<0) = E_R + [R_o(V_P + E_D - E_R)/(R_P + R_o)], \quad \text{(A4)}$$

and written in terms of δ as

$$V^b = [V_P\delta + E_R + E_D\delta]/(1 + \delta). \quad \text{(A5)}$$

Derivation of change in patch current and cell potential, after channel opens. At $t = 0$, it will be assumed that a channel has opened up in the patch and that provided there is a suitable driving force, the resulting current will depolarize the cell membrane potential. For $t \geq 0$, the total current flowing through the patch-clamp amplifier, i_T, will be given by

$$i_T = i_P + i_{Pc} + i_{ch} + i_s, \quad \text{(A6)}$$

so that the total current, in terms of the current components flowing through the membrane patch, will be given by

$$i_T = -\frac{(V_P + E_D - V)}{R_P} - C_P\frac{d}{dt}(V_P - V) - \frac{(V_P + E_c - V)}{R_{\gamma c}} + i_s, \quad \text{(A7)}$$

where i_s, the seal leakage current, is given by

$$i_s = -V_P/R_s. \quad \text{(A8)}$$

Similarly, the total current, in terms of the components flowing through the rest of the cell, will be given by

$$i_T = -\frac{(V_P - E_R)}{R_o} - C_o\frac{dV}{dt} + i_s. \quad \text{(A9)}$$

From Eqs. A7–A9, the full final differential equation for the change of cell membrane potential with time will be given by

$$V_P\alpha + E = V(1 + \alpha) + \tau(dV/dt), \quad \text{(A10)}$$

where

$$\tau = R_o(C_o + C_P) \qquad E = E_D\delta + \beta E_c + E_R$$
$$\alpha = (R_o/R_p) + (R_o/R_{\gamma c}) \qquad \beta = R_o/R_{\gamma c}, \quad \text{(A11)}$$

so that

$$\alpha = \delta + \beta. \quad \text{(A12)}$$

The specific solution of the full equation (Eq. A10) is simply given by

$$V = (\alpha V_P + E)/(1 + \alpha). \quad \text{(A13)}$$

Try a trial solution $V = Ae^{at}$ as a solution for the homogeneous equation

$$\tau(dV/dt) + (1 + \alpha)V = 0. \quad \text{(A14)}$$

The full solution of Eq. A10 becomes

$$V = (\alpha V_P + E)/(1 + \alpha) + Ae^{-(1+\alpha)t/\tau}. \quad \text{(A15)}$$

From the boundary conditions ($t \leq 0$, $V = V^b$),

$$A = -\beta[V_P - E_R - E_D\delta + (1 + \delta)E_c]/[(1 + \delta)(1 + \alpha)]. \quad (A16)$$

Defining ΔV as the change in potential when the channel opens ($t \geq 0$)

$$\Delta V = V - V^b, \quad (A17)$$

it may be shown from Eqs. A5 and A15–A17 that

$$\Delta V = \theta[1 - e^{-(1+\alpha)t/\tau}], \quad (A18)$$

where

$$\theta = V_P\rho - \lambda \quad (A19)$$

$$\rho = \beta/[(1 + \alpha)(1 + \delta)] \quad (A20)$$

$$\lambda = [\beta/(1 + \alpha)][(E_R + E_D\delta)/(1 + \delta) - E_c]. \quad (A21)$$

Thus it can be seen that for large positive values of V_P and inward currents, the membrane potential of the cell will be considerably depolarized.

Derivation of time taken to depolarize cell to action potential threshold. Provided that the size of the membrane patch is not too small in comparison with the rest of the cell and V_P is large enough, this depolarizing potential change could reach the threshold value necessary to initiate an action potential. Assuming that the change in potential necessary to reach threshold is V_{th}, the initiation time, t_i, that the channel needs to be open for this value to be reached and cause an action potential to be initiated can be obtained by solving the equation

$$V_{th} = \theta[1 - e^{-(1+\alpha)t_i/\tau}]. \quad (A22)$$

Hence

$$t_i = \left[\frac{\tau}{(1 + \alpha)}\right] ln\left[\frac{1}{1 - (V_{th}/\theta)}\right]. \quad (A23)$$

It may immediately be seen from Eq. A23 that if $\theta \leq V_{th}$, an action potential can never be initiated by this channel opening on its own. This corresponds to

$$[V_P\rho + \lambda] \leq V_{th}.$$

As far as the patch-clamp currents are concerned, they can be calculated by substituting for V from Eq. A15 into Eq. A9. The change in current after the channel opening Δi_T, will then be given by

$$\Delta i_T = i_T - i_T^b \quad (A24)$$

and Δi_T may be shown to be given by

$$\Delta i_T(t) = -(\theta/R_o)\{1 - [1 - (1 + \alpha)R_oC_o/\tau]e^{-(1+\alpha)t/\tau}\}. \quad (A25)$$

At $t = 0$, corresponding to the opening of the channel, the change in current, $\Delta i_T(0)$, will be given by

$$\Delta i_T(0) = -\gamma_c[(V_P - E_R - E_D\delta)/(1 + \delta) + E_c] \cdot [C_o/(C_o + C_P)]. \quad (A26)$$

The decrease in current with time during the opening of the channel as expressed by Eq. A25 is due to the increase in cell membrane potential opposing the driving force across the channel.

For relatively large cell/patch ratios, $\delta \rightarrow 0$ and $[C_o/(C_o + C_P)] \rightarrow 1$,

$$\Delta i_T(0) = \Delta i_T(t) = -\gamma_c(V_P - E_R + E_c) \quad (A27)$$

will tend to be constant and independent of time, with E_R and E_c representing the resting potential and channel null potential in each case defined with respect to the external solution.

APPENDIX B

Determination of the null potential and single-channel conductance of a channel for an intact patch in a very small cell

For large cells and relatively small patches, the change in total patch current Δi_T measured during the opening of a channel of conductance γ_c and resistance $R_{\gamma c}$ at a patch potential V_P and cell resting potential E_R results in $R_{\gamma c}$ given by

$$R_{\gamma c} = -[1/\Delta i_T(t)]\,[V_P - E_R + E_c] \quad (B1)$$

with

$$E_c = E_R - V_P^o, \quad (B2)$$

where E_c is the actual null or reversal potential of the channel and V_P^o is the value of patch potential at which $\Delta i_T = 0$.

However, for the case of intact patches in very small cells, such equations are quite inadequate. If the initial value of current is used (i.e., at $t = 0$), before current droop becomes significant, then $\Delta i_T(0)$ is given by Eq. A26 in Appendix A as

$$\Delta i_T(0) = -\gamma_c[(V_P - E_R - E_D\delta)/(1 + \delta) + E_c] \cdot [C_o/(C_o + C_P)]. \quad (B3)$$

Setting $\Delta i_T(0) = 0$, $V_P = V_P^o$,

$$E_c = (E_R + E_D\delta - V_P^o)/(1 + \delta). \quad (B4)$$

At any other value of V_P and Δi_T, using this value of E_c,

$$R_{\gamma c} = -(1/\Delta i_T)\,[(V_P - E_R - E_D\delta)/(1 + \delta) + E_c] \cdot [C_o/(C_o + C_P)]. \quad (B5)$$

If the composition of the pipette solution is very similar to that of the internal solution of the cell, as was the case in this paper, $E_D \approx 0$. In such a case,

$$E_c = (E_R - V_P^o)/(1 + \delta) \quad (B6)$$

and

$$R_{\gamma c} = -(1/\Delta i_T)\,[(V_P - E_R)/(1 + \delta) + E_c] \cdot [C_o/(C_o + C_P)]. \quad (B7)$$

Obviously, as cell size increases, $\delta \rightarrow 0$ and $C_o/(C_o + C_P) \rightarrow 1$, so that the two equations simplify even further to Eqs. B1 and B2. Eqs. B6 and B7 were used in the accompanying paper to calculate the E_c and $R_{\gamma c}$.

APPENDIX C

Derivation of the current spike in membrane patch due to an action potential in the rest of a very small cell

An action potential in the rest of a cell induces a change in the current flowing across the membrane patch. The equations to describe this situation will now be derived. The electrical circuit (Fig. C1) will be essentially the same as that of Fig. A1 in Appendix A, except that the circuit of the rest of the cell has been replaced by a "black box" voltage generator with voltage $V(t)$ and derivative dV/dt. The voltage from the time of opening of the channel ($t = 0$) until the action potential threshold is reached (t_i) will be given by the equations in Appendix A, whereas the voltage during the action potential will be digitally emulated from the digitization of a published waveform of an action potential recorded in a larger olfactory cell.

After the opening of the cation channel, at $t = 0$, the currents through the patch elements will be given (cf. Eqs. A6–A8) by

$$i_T = i_P + i_{Pc} + i_{ch} + i_s \tag{C1}$$

$$i_P = -[V_P + E_D - V(t)]/R_P \tag{C2}$$

$$i_{ch} = -[V_P + E_c - V(t)]/R_{\gamma c} \tag{C3}$$

$$i_{Pc} = -C_P \frac{d}{dt}[V_P - V(t)] = C_P \frac{dV(t)}{dt}, \tag{C4}$$

so that the total current flowing through the patch will become

$$i_T = -[V_P + E_D - V(t)]/R_P - [V_P + E_c - V(t)]/R_{\gamma c} + C_P dV(t)/dt + i_s. \tag{C5}$$

Hence the change in current through the patch after an opening of the cation channel will be given by

$$\Delta i_T = i_T - i_T^b, \tag{C6}$$

where (see Eq. A2)

$$i_T^b = i_s - \delta[V_P + E_D - E_R]/[R_o(1 + \delta)]. \tag{C7}$$

Before and up to the initial channel opening the membrane potential will be given by

$$V(t \leq 0) = (V_P \delta + E_R + E_D \delta)/(1 + \delta). \tag{C8}$$

From the initial opening of the channel until the initiation of the action potential, $V(t)$ will be given by Eqs. A15 and A16. It will be assumed that there is a threshold voltage value V_{th} above V^b. Similarly, the value of dV/dt can be calculated during this time by differentiating Eqs. A15 and A16. From this time on, it then simply becomes a question of choosing an appropriate function for the action potential. In practice, this was done by graphically digitizing the published waveform of an action potential recorded in an olfactory cell under whole-cell clamp conditions (Fig. 2 *A* in Anderson and Hamilton, 1987). The values were taken from the threshold point to a point beyond the undershoot. The values of dV/dt were calculated numerically as $[V(n + 1) - V(n)]/(2*\Delta t)$ for the value at the threshold point and as $[V(n + 1) - V(n - 1)]/(2*\Delta t)$ for the nth point thereafter. At the termination of this set of values, the channel was assumed to close and Δi_T to return to its 0 value. The values were scaled to span points from the threshold value to an overshoot of V_o, taken to be +20 mV.

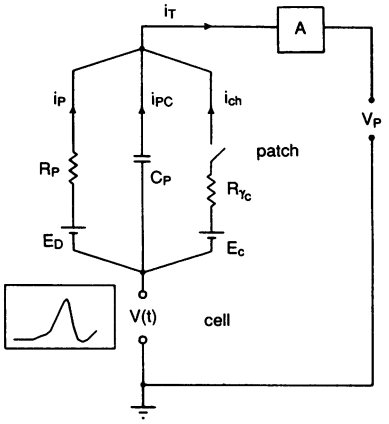

FIGURE C1 A schematic diagram of the electrical circuit of a membrane patch with a channel that can be in either an open or closed state. It is similar to part of Fig. A1, except that the rest of the cell component has simply been replaced by a "black box" voltage generator $V(t)$. For values before the action potential threshold the actual values of $V(t)$ and $dV(t)/dt$ were calculated from Eqs. A15–A21 in Appendix A. After the threshold, the potential was generated from a previously measured action potential waveform by scaling those values as described in the text. The symbols are the same as in Fig. A1.

We would like to thank Dr. Graham Bell for stimulating our interest in this area and for demonstrating the dissection of olfactory epithelia. We would also like to acknowledge our appreciation to Dr. Nino Quartararo, who wrote the original version of the basic channel record reading program and to Professor Elspeth McLachlan and Drs. Graham Bell and Chris French for constructive criticisms of the manuscript.

The financial support of the Australian National Health and Medical Research Council and the Australian Research Grants Scheme during the course of this work is also very much appreciated.

Received for publication 21 September 1988 and in final form 29 December 1988.

REFERENCES

Anderson, P. A. V., and K. A. Hamilton. 1987. Intracellular recordings from isolated salamander olfactory receptor neurons. *Neuroscience.* 21:167–173.

Anholt, R. R. H. 1987. Primary events in olfactory reception. *Trends Biochem. Sci.* 12:58–62.

Ashcroft, F. M., D. E. Harrison, and S. J. Ashcroft. 1984. Glucose induces closure of single potassium channels in isolated pancreatic beta cells. *Nature (Lond.).* 312:446–448.

Dionne, V. 1987. Membrane conductance mechanisms of dissociated cells from the olfactory epithelium of the mudpuppy, *Necturus maculosus. Ann. NY Acad. Sci.* 510:258–259.

Fenwick, E. M., A. Marty, and E. Neher. 1982. A patch-clamp study of bovine chromaffin cells and of their sensitivity to acetylcholine. *J. Physiol. (Lond.).* 331:577–597.

Firestein, S., and F. S. Werblin. 1987. Gated currents in isolated olfactory receptor neurons of the larval tiger salamander. *Proc. Natl. Acad. Sci. USA.* 84:6292–6296.

Fischmeister, R., R. K. Ayer, and R. L. DeHaan. 1986. Some limitations of the cell-attached patch clamp technique: a two-electrode analysis. *Pfluegers Arch. Eur. J. Physiol.* 406:73–82.

Frings, S., and B. Lindemann. 1988. Odorant response of isolated olfactory receptor cells is blocked by amiloride. *J. Membr. Biol.* 105:233–243.

Gesteland, R. C. 1986. Speculations on receptor cells as analyzers and filters. *Experientia (Basel).* 42:287–291.

Gesteland, R. C. 1988. Receptor impulse interval patterns define equivalent olfactory stimuli. *Soc. Neurosci. Abstr.* 14:1200.

Getchell, T. V. 1986. Functional properties of vertebrate olfactory receptor neurons. *Physiol. Rev.* 66:772–818.

Getchell, T. V., and G. M. Shepherd. 1978. Adaptive properties of olfactory receptors analysed with odour pulses of varying duration. *J. Physiol. (Lond.).* 282:541–560.

Hamill, O. P., A. Marty, E. Neher, B. Sakmann, and F. S. Sigworth. 1981. Improved patch-clamp techniques for high resolution current recording from cells and cell-free membrane patches. *Pfluegers Arch. Eur. J. Physiol.* 391:85–100.

Hedlund, B., L. M. Masukawa, and G. M. Shepherd. 1987. Excitable properties of olfactory receptor neurons. *J. Neurosci.* 7:2338–2343.

Labarca, P., S. A. Simon, and R. H. Anholt. 1988. Activation by odorants of a multistate cation channel from olfactory cilia. *Proc. Natl. Acad. Sci. USA.* 85:944–947.

Lancet, D. 1986. Vertebrate olfactory reception. *Annu. Rev. Neurosci.* 9:329–355.

Lancet, D., and U. Pace. 1987. The molecular basis of odor recognition. *Trends Biochem. Sci.* 12:63–66.

Maue, R. A., and V. Dionne. 1987*a*. Preparation of isolated mouse olfactory receptor neurons. *Pfluegers Arch. Eur. J. Physiol.* 409:244–250.

Maue, R. A., and V. Dionne. 1987*b*. Patch-clamp studies of isolated mouse olfactory receptor neurons. *J. Gen. Physiol.* 90:95–125.

Moulton, D. G. 1977. Minimum odorant concentrations detectable by the dog and their implications for olfactory receptor sensitivity. *In* Chemical Signals in Vertebrates. D. Muller-Schwarze and M. Mozell, editors. Plenum Publishing Corp., New York. 455–464.

Nakamura, T., and G. H. Gold. 1987. A cyclic nucleotide-gated conductance in olfactory receptor cilia. *Nature (Lond.).* 316:442–444.

Sakmann, B., and G. Trube. 1984. Conductance properties of single inwardly rectifying potassium channels in ventricular cells from guinea-pig heart. *J. Physiol. (Lond.).* 347:641–657.

Suzuki, N. 1987. Voltage-dependent conductances in solitary olfactory receptor cells. *Ann. NY Acad. Sci.* 510:647–648.

Trotier, D. 1986. A patch-clamp analysis of membrane currents in salamander olfactory cells. *Pfluegers Arch. Eur. J. Physiol.* 407:589–595.

Trotier, D., and P. MacLeod. 1987. The amplification process in olfactory receptor cells. *Ann. NY Acad. Sci.* 510:677–679.